Journal of Applied Geophysics 150 (2018) 144–152

Contents lists available at ScienceDirect

Journal of Applied Geophysics

journal homepage: www.elsevier.com/locate/jappgeo

A novel 2.5D finite difference scheme for simulations of resistivity logging in anisotropic media

Shubin Zeng, Fangzhou Chen, Dawei Li, Ji Chen, Jiefu Chen*

Department of Electrical and Computer Engineering, University of Houston, USA

ARTICLE INFO

Article history:
Received 20 June 2017
Received in revised form 29 October 2017
Accepted 20 January 2018
Available online 31 January 2018

Keywords:
2.5D finite difference method
Resistivity logging
Anisotropy

ABSTRACT

The objective of this study is to develop a method to model 3D resistivity well logging problems in 2D formation with anisotropy, known as 2.5D modeling. The traditional 1D forward modeling extensively used in practice lacks the capability of modeling 2D formation. A 2.5D finite difference method (FDM) solving all the electric and magnetic field components simultaneously is proposed. Compared to other previous 2.5D FDM schemes, this method is more straightforward in modeling fully anisotropic media and easy to be implemented. Fourier transform is essential to this FDM scheme, and by employing Gauss-Legendre (GL) quadrature rule the computational time of this step can be greatly reduced. In the numerical examples, we first demonstrate the validity of the FDM scheme with GL rule by comparing with 1D forward modeling for layered anisotropic problems, and then we model a complicated 2D formation case and find that the proposed 2.5D FD scheme is much more efficient than 3D numerical methods.

1. Introduction

Nowadays, directional drilling is of great interests to hydrocarbon exploration. Alongside with the directional drilling, the accurate geological boundary detection is vital to successful well drilling (Omeragic et al., 2009; Bittar and Aki, 2015; Zhou, 2015). Different deep directional resistivity tools (Li et al., 2005; Bittar et al., 2009) have been proposed and applied to pro-active well placement to accurately position the wellbore with respect to geological boundary. These propagation tools usually operate at frequencies from kilohertz to megahertz. After analyzing the tool responses of transmitter-receiver (T-R) pairs transmitted in real-time or obtained after drilling, the subsurface formation can be reconstructed at ground station and help to make geosteering decisions. Many forward modeling methods for resistivity well logging tool in complex subsurface formations, for instance, conventional numerical schemes such as finite difference method (FDM) (Abubakar et al., 2008; Davydycheva, 2010), finite element method (FEM) (Nam et al., 2012) and method of integral equations (IE) (Abubakar et al., 2006a), or methods specifically designed for this application (Chen et al., 2016), have been carried out to provide promising forward modeling. FDM has gained its popularity by its easy implementation while FEM is capable to model complex geometry accurately and IE can achieve a higher level of accuracy due to its implementation of Green's function.

Popular analytical 1D model (Zhong et al., 2008; He et al., 2015) assumes that the formation is layered structure with transverse isotropic (TI) media. Inside each layer, the resistivity can be characterized by the horizontal resistivity R_h and vertical resistivity R_v. The principal axis associated with R_v is assumed to be perpendicular to each boundary. By utilizing explicit formulas based on reflection and transmission coefficients (Huang and Shen, 1989) and fast Hankel transform (FHT) (Anderson, 1979), the solution for the 1D model can be calculated very fast and provides a possibility to build real-time inversion. However, more often, faults, unconformities and other lateral changes appear underground because of the earth movements. 1D fast forward solver is no longer practicable in modeling such complex formation, not to mention model fully anisotropy.

There are many methods devoted to the numerical solutions to Maxwell's equations in complex formations, in the context of geosteering, controlled-source EM (CSEM) and other related problems. The employment of popular FDM starts with the pioneering work of Yee (1966), in which staggered grids are introduced. Later the FDM is generalized into 3D fully anisotropic media (Weidelt, 1999; Wang and Fang, 2001; Weiss and Newman, 2002; Hou et al., 2006; Liu and Yin, 2014). FD forward solver can also be modeled on a Lebedev grid (Lebedev, 1964; Davydycheva et al., 2003; Jaysaval et al., 2016). Though this gird can model fully anisotropy more accurately, the computation cost is increased fourfold as compared to Yee's grid. The more flexible but involved

* Corresponding author.
E-mail address: jchen84@uh.edu (J. Chen).

https://doi.org/10.1016/j.jappgeo.2018.01.021
0926-9851/

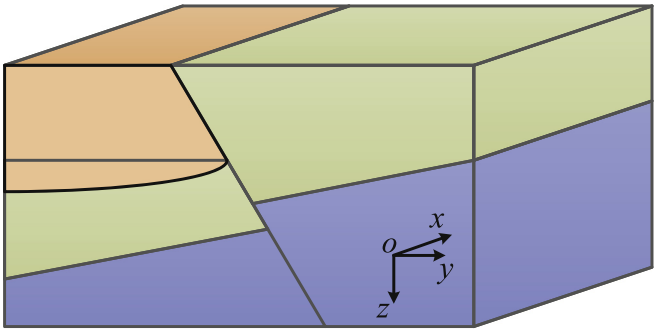

Fig. 1. A 2D underground formation consisting fault and unconformity with *x*-axis (north) as the strike direction.

finite element method has also been developed (Jin et al., 1999; Li and Key, 2007; Kong et al., 2007). The integral equation (IE) method (Hursan and Zhdanov, 2002; Zhdanov et al., 2006) only requires discretization at the region of anomaly or along the interfaces, thus leading to a much smaller number of unknowns. However, IE needs solving a full matrix equation, and accurate computation of Green's function for the inhomogeneous background media is tedious and nontrivial.

One should note that, despite the fact that 3D forward modeling (Wang and Fang, 2001; Weiss and Newman, 2002; Davydycheva et al., 2003; Avdeev, 2005; Hou et al., 2006) combining high performance computing is available both in academic researches and commercial softwares, fully 3D methods which must discretize the computation domain into numerous elements are still prohibitively expensive for fast forward modeling, not to mention the inversion requiring repeatedly calling of forward modeling. An intermediate solution between 1D TI model and fully 3D model is the 2D model which has uniform property along the strike axis. Even taking geological deformation into consideration, it is reasonable to assume that, within the detection range of a typical EM geosteering tool (centimeters to tens of meters) the geological formation is a 2D structure, which exhibits uniform EM properties in strike direction. A general formation with fault and unconformity which shows uniformity in the *x*-direction but inhomogeneity in the *y*-*z* plane, is shown in Fig. 1. Generally speaking, the transmitter of the EM tool consists of electric current coils and so is the receiver. By utilizing EM theory, the current coils can be modeled as magnetic dipoles if the dimension of coils is small compared to the surrounding formation. Such a 2D structure with an arbitrary oriented magnetic dipole source radiating around is usually known as 2.5D problem. In order to make use of the 2D structure to reduce the number of unknowns, Fourier transform technique can be applied to transform the magnetic dipole source into a set of line current sources along the strike direction such that the problem goes into spectral domain with complete 2D property. Compared to 3D solver, this brings mathematical simplicity to the problem and substantially reduces the number of unknowns and computational cost. Different methods, including FDM (Abubakar et al., 2006b; Chen et al., 2011), FEM (Li and Key, 2007; Key and Ovall, 2011) and IE method (Dyatlov et al., 2015, 2017), have been applied to model 2.5D problem. Though these methods are able to model complex 2D formation, the fully anisotropy of the formation has seldom been discussed and simulated. The forward modeling of 2.5D problem is also essential to the fast inversion of 2D formation for various applications (Abubakar et al., 2005; Key, 2016).

Considering the accuracy requirement for practical application and the implemented complexity of the schemes, we intend to apply FDM to model EM propagation tools in 2D formation with fully anisotropy. To the best knowledge of authors, fast solver for 2.5D problem involving fully anisotropic formation in resistivity logging has not been developed in previous publications. In this paper, we focus on developing a scheme to model the responses of resistivity logging tools in a 2D underground formation by employing the algorithm of 2.5D FDM. The rest of this paper is organized as follows. The statement of the problem is presented first in Section 2. The formulations for 2.5D FDM modeling are presented in Section 3, which is followed by the discussion of numerical integration methods in Section 4. Then, numerical examples are exhibited in Section 5. Finally, the conclusion is drawn in Section 6.

2. Problem statement

Before we develop the methodology applied to model 2.5D problem, we begin by declaring the formation model and presenting the governing differential equations to model electromagnetic exploration.

In this paper, we consider a 2D conductive structure with fully anisotropic conductivity and let *x*-axis be the structural strike direction. The global coordinate for 2D structure is right-handed with *y*-axis towards east and *z*-axis pointing directly down. The geological formation model at each point is assumed to has fully anisotropic electric conductivity tensor $\overline{\boldsymbol{\sigma}}$ and is uniform along the strike direction. Just as the structure shown in Fig. 1, the media can be decomposed into D domains $\Omega(d), d = 1, 2, \ldots, D$, with each domain having constant conductivity tensor $\overline{\boldsymbol{\sigma}}(d)$. Here, the conductivity tensor

$$\overline{\boldsymbol{\sigma}} = \begin{bmatrix} \sigma_{xx} & \sigma_{xy} & \sigma_{xz} \\ \sigma_{yx} & \sigma_{yy} & \sigma_{yz} \\ \sigma_{zx} & \sigma_{zy} & \sigma_{zz} \end{bmatrix} \tag{1}$$

is fully anisotropic but symmetric and positive definite. Hence, after three Euler's elementary rotations (Fig. 2), the conductivity tensor can be rotated into its three principal axes (x''', y''', z''') and diagonalized (Martí, 2014). This property provides a distinct way to specify the conductivity tensor with six parameters

$$\overline{\boldsymbol{\sigma}} = \boldsymbol{R}_z^T(\alpha_s)\boldsymbol{R}_x^T(\alpha_d)\boldsymbol{R}_z^T(\alpha_l) \begin{bmatrix} \sigma_{x'''} & 0 & 0 \\ 0 & \sigma_{y'''} & 0 \\ 0 & 0 & \sigma_{z'''} \end{bmatrix} \boldsymbol{R}_z(\alpha_l)\boldsymbol{R}_x(\alpha_d)\boldsymbol{R}_z(\alpha_s) \tag{2}$$

where $\boldsymbol{R}_z(\alpha_l)$, $\boldsymbol{R}_x(\alpha_d)$, and $\boldsymbol{R}_z(\alpha_s)$ are the rotation matrices and superscript T denotes transpose. α_s (anisotropy strike), α_d (anisotropy dip) and α_l (anisotropy slant) are the specific Euler's rotation angles. Generally, rotation matrix $\boldsymbol{R}_e(\alpha_f)$ ($e = x, z$ and $f = s, d, l$) denotes the rotation transformation around the e-axis by angle α_f. $\sigma_{x'''}$, $\sigma_{y'''}$ and $\sigma_{z'''}$ are the three conductivity components along the principal directions. Fig. 2 shows how to rotate the fully anisotropic conductivity tensor $\overline{\boldsymbol{\sigma}}$ into the diagonalized tensor by successively applying three rotation transformations corresponding to the three Euler's angles.

To apply FDM to model propagation tools in 2D formation, we formulate the electromagnetic problem in the frequency domain with a temporal-dependence of $e^{-i\omega t}$, where $i^2 = -1$ and ω is the angular frequency. The governing equations to solve the electric and magnetic field vectors can be obtained from Maxwell's curl equations. Assuming that there exists both electric current source $\mathbf{J}$ and magnetic current source $\mathbf{M}$ in the excitation of electromagnetic propagation tool, we have

$$\nabla \times \mathbf{H}(\mathbf{r}) + i\omega \left(\epsilon(\mathbf{r}) + i\frac{\overline{\boldsymbol{\sigma}}(\mathbf{r})}{\omega} \right) \cdot \mathbf{E}(\mathbf{r}) = \mathbf{J}(\mathbf{r}), \tag{3}$$

$$\nabla \times \mathbf{E}(\mathbf{r}) - i\omega\mu(\mathbf{r})\mathbf{H}(\mathbf{r}) = \mathbf{M}(\mathbf{r}) \tag{4}$$

where $\mathbf{r} \equiv x\hat{\mathbf{x}} + y\hat{\mathbf{y}} + z\hat{\mathbf{z}}$, $\mathbf{E} \equiv E_x\hat{\mathbf{x}} + E_y\hat{\mathbf{y}} + E_z\hat{\mathbf{z}}$ and $\mathbf{H} \equiv H_x\hat{\mathbf{x}} + H_y\hat{\mathbf{y}} + H_z\hat{\mathbf{z}}$ denote the position, electric field and magnetic field vectors,

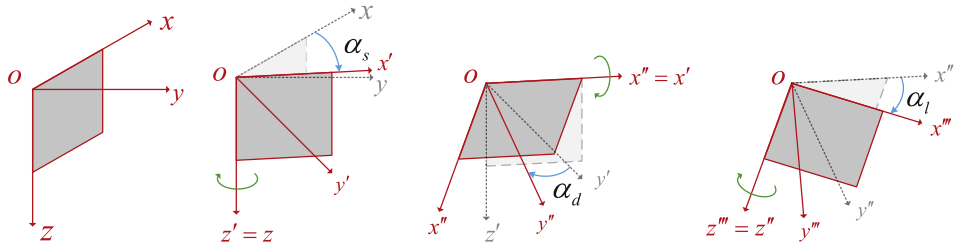

Fig. 2. Illustration of three successive rotation transformations using anisotropic strike (α_s), dip (α_d) and slant (α_l) angles, to capture the principal axes of the fully anisotropic media.

respectively. $\mu(\mathbf{r})$ is the magnetic permeability and assumed to be the free space value μ_0. $\epsilon(\mathbf{r})$ is the electric permittivity and assumed to be scalar function invariant along the structural strike direction. $\mathbf{J} = J_x\hat{\mathbf{x}} + J_y\hat{\mathbf{y}} + J_z\hat{\mathbf{z}}$ and $\mathbf{M} = M_x\hat{\mathbf{x}} + M_y\hat{\mathbf{y}} + M_z\hat{\mathbf{z}}$ denote electric and magnetic current sources, respectively.

3. 2.5D FDM for fully anisotropic EM modeling

To derive the 2.5D FDM algorithm to model EM propagation tool in 2D fully anisotropic formation, we can simplify the current on the transmitter coil as magnetic dipole, i.e., $\mathbf{M}(\mathbf{r}) = M\delta(\mathbf{r} - \mathbf{r}'_M)\hat{\mathbf{e}}_{Ms}$, where $\mathbf{r}'_M$ is the central position of the dipole and $\hat{\mathbf{e}}_{Ms}$ is the unit direction of the dipole. The basic idea behind 2.5D FDM is to convert field vectors and source vectors into spectral domain by Fourier transform along the strike direction so as to reduce the 3D problem into a sequence of 2D problems. The 1D spatial Fourier transform and its normalized inverse transform with respect to the x-axis are

$$\tilde{\mathbf{u}}(k_x, y, z) = \int_{-\infty}^{\infty} \mathbf{u}(x, y, z) e^{ik_x x} dx \,, \tag{5}$$

and

$$\mathbf{u}(x, y, z) = \frac{1}{2\pi} \int_{-\infty}^{\infty} \tilde{\mathbf{u}}(k_x, y, z) e^{-ik_x x} dk_x \,. \tag{6}$$

By applying Fourier transform to Eqs. (3) and (4), we obtain

$$\tilde{\nabla} \times \tilde{\mathbf{H}}(\mathbf{r}) + i\omega \left(\epsilon(\mathbf{r}) + i\frac{\overline{\boldsymbol{\sigma}}(\mathbf{r})}{\omega} \right) \cdot \tilde{\mathbf{E}}(\mathbf{r}) = \mathbf{0} \,, \tag{7}$$

$$\tilde{\nabla} \times \tilde{\mathbf{E}}(\mathbf{r}) - i\omega\mu(\mathbf{r})\tilde{\mathbf{H}}(\mathbf{r}) = \tilde{\mathbf{M}}(\mathbf{r}) \tag{8}$$

where $\tilde{\nabla} \equiv \hat{\mathbf{x}}(ik_x) + \hat{\mathbf{y}}\partial_y + \hat{\mathbf{z}}\partial_z$. The electric current source is omitted to make the discussion concisely. In fact, if one needs to handle the electric current source, it can be added to the final right-hand side vector straightforward with little computational penalty.

Using the definitions of dot product between tensors and vectors and curl operations in Eqs. (7) and (8), we can obtain

$$\begin{cases} \partial_y \tilde{H}_z - \partial_z \tilde{H}_y + i\omega\epsilon\tilde{E}_x \\ \quad - \left(\sigma_{xx}\tilde{E}_x + \sigma_{xy}\tilde{E}_y + \sigma_{xz}\tilde{E}_z \right) = 0 \,, \\ \partial_z \tilde{H}_x - ik_x\tilde{H}_z + i\omega\epsilon\tilde{E}_y \\ \quad - \left(\sigma_{yx}\tilde{E}_x + \sigma_{yy}\tilde{E}_y + \sigma_{yz}\tilde{E}_z \right) = 0 \,, \\ ik_x\tilde{H}_y - \partial_y \tilde{H}_x + i\omega\epsilon\tilde{E}_z \\ \quad - \left(\sigma_{zx}\tilde{E}_x + \sigma_{zy}\tilde{E}_y + \sigma_{zz}\tilde{E}_z \right) = 0 \,, \end{cases} \tag{9}$$

and

$$\begin{cases} \partial_y \tilde{E}_z - \partial_z \tilde{E}_y - i\omega\mu\tilde{H}_x = \tilde{M}_x \,, \\ \partial_z \tilde{E}_x - ik_x\tilde{E}_z - i\omega\mu\tilde{H}_y = \tilde{M}_y \,, \\ ik_x\tilde{E}_y - \partial_y \tilde{E}_x - i\omega\mu\tilde{H}_z = \tilde{M}_z \,. \end{cases} \tag{10}$$

Note that the nine conductivity components are defined in the global Cartesian coordinate system which is not the principal axis coordinate system of the media. The outmost boundaries of the computational domain are located sufficiently far away from the current sources to guarantee negligible reflections because of the exponential decay of the EM field in lossy media, such that the homogeneous Dirichlet boundary condition can be enforced at the outmost boundaries with negligible loss of computational accuracy. We can observe that the derivatives with respect to x are replaced by analytical expression of ik_x in Eqs. (9) and (10). Hence, for each specific k_x, one only need to make a 2D finite difference discretization.

One possible scheme to solve the EM fields is to eliminate $\tilde{E}_x$ and $\tilde{H}_x$ and solve the tangential components of the EM fields. At first glance, this scheme can reduce the number of unknowns by one third. However, it is not trivial to eliminate the longitudinal fields in the strike direction when the formation is fully anisotropic. Meanwhile, by reducing the total number of unknowns, it will increase the number of nonzero entries in each row in the final system matrix, resulting in similar computation cost for direct sparse matrix solver. In fact, we compared the scheme using four components ($\tilde{E}_y$, $\tilde{E}_z$, $\tilde{H}_y$, $\tilde{H}_z$) and the scheme using six components ($\tilde{E}_x$, $\tilde{E}_y$, $\tilde{E}_z$, $\tilde{H}_x$, $\tilde{H}_y$, $\tilde{H}_z$). As a result, the solution time of the scheme using six components is less than half of the scheme using four components for the same grid discretization and sparse matrix direct solver.

The same problem may reside in the scheme (Abubakar et al., 2008; Chen et al., 2011) in which magnetic field $\tilde{\mathbf{H}}$ is eliminated from Eqs. (7) and (8) to obtain

$$\tilde{\nabla} \times \tilde{\nabla} \times \tilde{\mathbf{E}}(\mathbf{r}) - \left[i\omega\mu(\mathbf{r})\overline{\boldsymbol{\sigma}}(\mathbf{r}) + \omega^2\mu(\mathbf{r})\epsilon(\mathbf{r}) \right] \tilde{\mathbf{E}}(\mathbf{r}) = \tilde{\nabla} \times \tilde{\mathbf{M}}(\mathbf{r}) \,. \tag{11}$$

Moreover, in Eq. (11), the curl operator of magnetic current and the curl calculation of electric field to obtain the magnetic field by Eq. (7) tend to contaminate the accuracy of the calculated field. Hence, in this work, we will directly employ FDM to discretize Eqs. (9) and (10) to solve all the components of EM field simultaneously.

We apply the FD scheme with a Cartesian Yee's grid shown in Fig. 3 to discretize the truncated 2D plane whose outmost boundary is far away from source. The 2D Yee's grid can be regarded as a 3D discretization with the grid size along the strike direction approaching zero such that the derivatives with respect to x are replaced by an analytical expression ik_x. To solve the equations efficiently, the computational domain is discretized using combination of uniform grids in the inner computational space between transmitter and receiver and nonuniform grids for the remaining space. With the

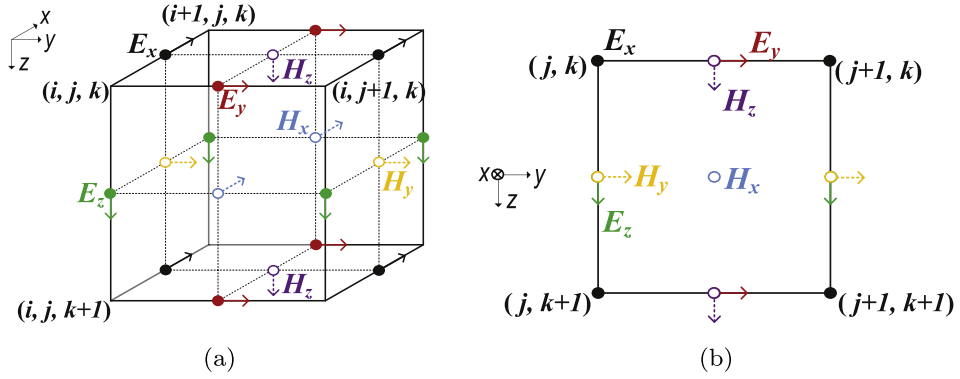

Fig. 3. Staggered Yee's grid used for FDM simulation: (a) a 3D grid and (b) a compact 2D slice.

reduced Yee's grid system shown in Fig. 3b, Eqs. (9) and (10) can be discretized as

$$\begin{cases} \frac{1}{\Delta y(j,k)}\left[\tilde{H}_z\left(j+\frac{1}{2},k\right)-\tilde{H}_z\left(j-\frac{1}{2},k\right)\right] \\ \quad -\frac{1}{\Delta z(j,k)}\left[\tilde{H}_y\left(j,k+\frac{1}{2}\right)-\tilde{H}_y\left(j,k-\frac{1}{2}\right)\right] \\ \quad +i\omega\epsilon\tilde{E}_x(j,k)-\left[\sigma_{xx}\tilde{E}_x(j,k)+\sigma_{xy}\tilde{E}_y(j,k)+\sigma_{xz}\tilde{E}_z(j,k)\right]=0\,, \\ \frac{1}{\Delta z\left(j+\frac{1}{2},k\right)}\left[\tilde{H}_x\left(j+\frac{1}{2},k+\frac{1}{2}\right)-\tilde{H}_x\left(j+\frac{1}{2},k-\frac{1}{2}\right)\right] \\ \quad -ik_x\tilde{H}_z\left(j+\frac{1}{2},k\right)+i\omega\epsilon\tilde{E}_y\left(j+\frac{1}{2},k\right) \\ \quad -\left[\sigma_{yx}\tilde{E}_x\left(j+\frac{1}{2},k\right)+\sigma_{yy}\tilde{E}_y\left(j+\frac{1}{2},k\right)+\sigma_{yz}\tilde{E}_z\left(j+\frac{1}{2},k\right)\right]=0\,, \\ ik_x\tilde{H}_y\left(j,k+\frac{1}{2}\right)-\frac{1}{\Delta y\left(j,k+\frac{1}{2}\right)} \\ \quad \left[\tilde{H}_x\left(j+\frac{1}{2},k+\frac{1}{2}\right)-\tilde{H}_z\left(j-\frac{1}{2},k+\frac{1}{2}\right)\right]+i\omega\epsilon\tilde{E}_z\left(j,k+\frac{1}{2}\right) \\ \quad -\left[\sigma_{zx}\tilde{E}_x\left(j,k+\frac{1}{2}\right)+\sigma_{zy}\tilde{E}_y\left(j,k+\frac{1}{2}\right)+\sigma_{zz}\tilde{E}_z\left(j,k+\frac{1}{2}\right)\right]=0\,, \end{cases} \tag{12}$$

and

$$\begin{cases} \frac{1}{\Delta y\left(j+\frac{1}{2},k+\frac{1}{2}\right)}\left[\tilde{E}_z\left(j+1,k+\frac{1}{2}\right)-\tilde{E}_z\left(j,k+\frac{1}{2}\right)\right] \\ \quad -\frac{1}{\Delta z\left(j+\frac{1}{2},k+\frac{1}{2}\right)}\left[\tilde{E}_y\left(j+\frac{1}{2},k+1\right)-\tilde{E}_y\left(j+\frac{1}{2},k\right)\right] \\ \quad -i\omega\mu\tilde{H}_x\left(j+\frac{1}{2},k+\frac{1}{2}\right)=\tilde{M}_x\left(j+\frac{1}{2},k+\frac{1}{2}\right)\,, \\ \frac{1}{\Delta z\left(j,k+\frac{1}{2}\right)}\left[\tilde{E}_x(j,k+1)-\tilde{E}_x(j,k)\right]-ik_x\tilde{E}_z\left(j,k+\frac{1}{2}\right) \\ \quad -i\omega\mu\tilde{H}_y\left(j,k+\frac{1}{2}\right)=\tilde{M}_y\left(j,k+\frac{1}{2}\right)\,, \\ ik_x\tilde{E}_y\left(j+\frac{1}{2},k\right)-\frac{1}{\Delta y\left(j+\frac{1}{2},k\right)}\left[\tilde{E}_x(j+1,k)-\tilde{E}_x(j,k)\right] \\ \quad -i\omega\mu\tilde{H}_z\left(j+\frac{1}{2},k\right)=\tilde{M}_z\left(j+\frac{1}{2},k\right)\,, \end{cases} \tag{13}$$

where $\Delta y(m,n)=y\left(m+\frac{1}{2},n\right)-y\left(m-\frac{1}{2},n\right)$ and $\Delta z(m,n)=z\left(m,n+\frac{1}{2}\right)-z\left(m,n-\frac{1}{2}\right)$, respectively.

As we can observe from Eq. (12), the equations including general conductivity anisotropy will couple all the components of electric field together. However, the Yee's grid is staggered which means that three components of electric field vector are not defined at the same spatial position. For instance, if we need to solve the first equation of Eq. (12), the $\sigma_{xy}\tilde{E}_y$ and $\sigma_{xz}\tilde{E}_z$ terms are defined at the edge centers on the FD grids while the $\sigma_{xx}\tilde{E}_x$ term is defined at cell corners. Meanwhile, by using FDM, the material properties are assigned cell by cell so one cannot directly use the conductivity affiliated to single cell. In this work, we employed the weighed average method applied by Weiss and Newman (2002) which calculates the weighted value of all the adjacent cells of one node. In 2D case, the number of adjacent cells for electric field components is two for components $\tilde{E}_y$ and $\tilde{E}_z$ located at edge centered node and four for component $\tilde{E}_x$ located at corners.

Upon discretization and employment of the weighted average method, we can obtain the corresponding system linear equation for Eqs. (7) and (8), written in matrix notation as

$$\left(\tilde{\mathbf{A}}+ik_x\tilde{\mathbf{P}}\right)\cdot\tilde{\mathbf{X}}=\tilde{b}\,, \tag{14}$$

where $\tilde{\mathbf{A}}$ and $\tilde{\mathbf{P}}$ are the stiffness matrices resulting from the left side of Eqs. (7) and (8), $\tilde{\mathbf{X}}=[\tilde{E}_x,\tilde{E}_y,\tilde{E}_z,\tilde{H}_x,\tilde{H}_y,\tilde{H}_z]^T$ is a vector containing the electric and magnetic fields at all the nodes, and $\tilde{\mathbf{b}}=[0,0,0,\tilde{M}_x,\tilde{M}_y,\tilde{M}_z]^T$ is a vector resulting from magnetic dipole source. The matrix $\tilde{\mathbf{A}}$ is independent of wavenumber k_x while the matrix $ik_x\tilde{\mathbf{P}}$ is proportional to k_x. Once the FD grids are defined, the matrices $\tilde{\mathbf{A}}$ and $\tilde{\mathbf{P}}$ are fixed regardless of the value of k_x. This saves the computation time substantially for 2.5D FEM modeling which needs to solve a sequence of k_x.

The discretization of the 2D computation domain by FD scheme is similar to the method employed by Abubakar et al. (2008). The meshes for the inner region between the transmitter and receiver are dense and uniform while the boundaries are then extended away from the inner region by nonuniform meshes. The size of the uniform meshes depends on the conductivities of the formation, the tool spacing and the working frequency of the tool. The size of the nonuniform mesh grows with a constant ratio to reduce the number of unknowns but keep the accuracy of 2.5D FD scheme in the inner region. The mesh discretization is adaptive when the transmitters and receivers move in the 2D formation.

The total number of unknowns by 2.5D FDM is much smaller than that by a 3D discretization with a similar grid density. Thus, the resulting linear system equations in Eq. (14) can be solved by direct sparse matrix solver efficiently. One of the advantages for using direct solver is that the slow convergence and poor accuracy can be avoided. Using multifrontal LU decomposition method (Davis and Duff, 1997), one can solve for all the source excitations simultaneously. The multifrontal LU decomposition method we used is the UMFPACK solver, which is available in the SuiteSparse package (Davis, 2006). This feature provides an efficient solution for triaxial induction and LWD tools which have couple of transmitters and receivers. After the EM fields in spectral domain are solved for each k_x, one must apply inverse Fourier transform to obtain the corresponding spatial field values.

4. Numerical integration for inverse Fourier transform

The simulation time of the 2.5D FDM modeling not only depends on the computational complexity of the 2D modeling methodology, but also is proportional to the total number of quadrature points for

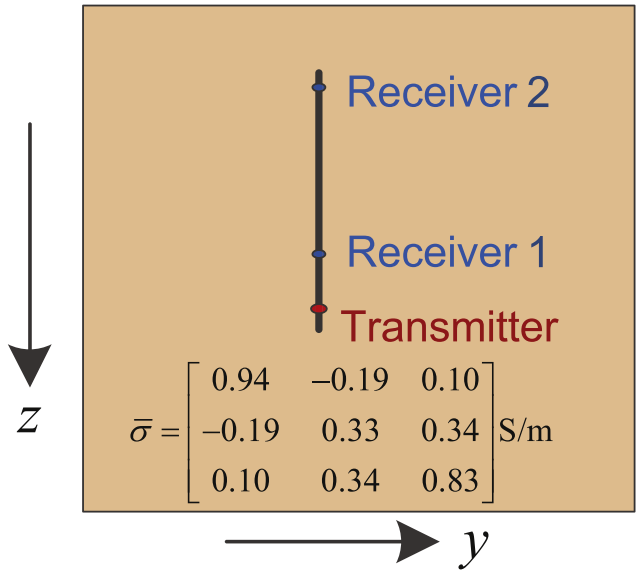

Fig. 4. A specific tool with one transmitter and two receivers is placed vertically in a homogeneous and fully anisotropic media. The T-R spacings are 0.56 and 2.44 m, respectively. The tool works at a frequency of 2 MHz.

inverse Fourier transform. When one tries to apply Eq. (6) to calculate the spatial fields, interpolatory quadrature methods, such as midpoint rule, trapezoid rule or Simpson's rule (Quarteroni et al., 2010), can be employed to do numerical integration over truncated integral range of k_x. However, interpolatory quadrature methods usually need to sample numerous points to acquire results with small relative errors. Besides interpolatory quadrature methods, Gaussian quadrature rules (Quarteroni et al., 2010), e.g., Gauss-Legendre (GL) rule and Gauss-Lobatto-Legendre (GLL) rule, are very attractive to do numerical integration over finite integral range due to their less requirements for sampling points. In this section, we will look into and compare different quadrature methods including midpoint rule, GL, and GLL scheme.

To compare the different numerical rules, we begin with studying the spectral behaviors of a specific tool with one transmitter and two receivers. The transmitter-receiver (T-R) offsets are 0.56 m and 2.44 m, respectively. Assuming that the tool is placed vertically inside a formation whose conductivity is homogeneous and fully anisotropic, we can apply 2.5D FDM to solve the spectral behavior of the magnetic field at the two receivers. As shown in Fig. 4, the conductivity tensor is symmetric and positive definite. Fig. 5a and b shows the real and imaginary parts of the magnetic field H_x at receivers 1 and 2 in the k_x domain. The results show that the magnetic field approaches zero when k_x goes to negative and positive infinities. This observation makes sense because the wavenumber k in the formation is constant, providing a growing decay factor in wavenumber $k_\rho = \sqrt{k^2 - k_x^2}$ when k_x goes to negative and positive infinities. Hence the small part of the integrand $\tilde{\mathbf{u}}(k_x, y, z)$ whose magnitude is well below the tolerance, say, 10^{-3} of the magnitude at $k_x = 0$, can be neglected, while the calculated fields keep a reasonable accuracy. By this way, the numerical integration of the wavenumber k_x is truncated into $[k_{xm-}, k_{xm+}]$ with k_{xm-} and k_{xm+} representing the truncation points of the integral. Moreover, in order to improve the efficiency and accuracy, we employ numerical integration rules on real k_x axis by separating $[k_{xm-}, k_{xm+}]$ into negative region $[k_{xm-}, 0]$ and positive region $[0, k_{xm+}]$, in order to weaken the adverse effect of the oscillation near point $k_x = 0$.

Fig. 6 shows the accuracy of the numerical value of magnetic field at receiver 1 by employing midpoint rule, GL rule and GLL rule. The reference solutions utilize the results obtained by applying 1D code which is of high precision when solving the tool response in horizontally layered transverse isotropic media. In fact, the fully anisotropic conductivity tensor shown in Fig. 4 is transformed by rotating a diagonally transverse isotropic tensor. Hence, when setting up the 1D code, we can inversely rotate the tool in the same transverse isotropic and homogeneous media by the corresponding angles to obtain the same fully anisotropy with respect to the sonde coordinate. It is clearly shown in the comparison that the Gaussian rules perform much better than midpoint rule. Approximately, GL and GLL rules can acquire the same level of accuracy by only utilizing half of the sampling points used by midpoint rule. The results also show that about 20 sampling points are able to reach a relative error below 1%, no matter employing GL or GLL rule.

Although the illustration of numerical integration for inverse Fourier transform is based on homogeneous and fully anisotropic media, the GL and GLL rules are valid for complex formation as long as the formation is lossy. In the remaining numerical examples, we implemented GL rule to the inverse Fourier transform.

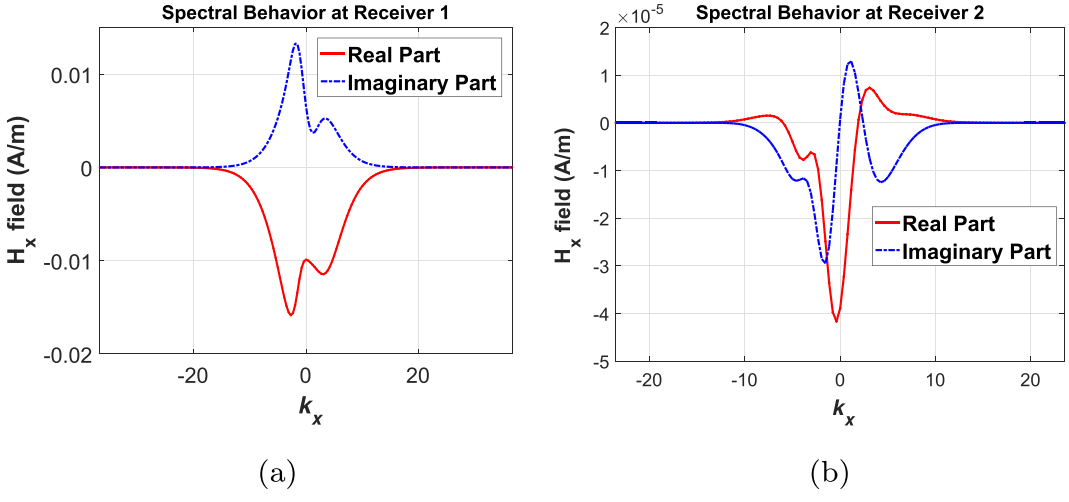

Fig. 5. The spectral behavior of the x-components of the magnetic fields at two receivers when transmitter has x-directed unit magnetic dipole moment: (a) real part and imaginary part of H_x at receiver 1; (b) real part and imaginary part of H_x at receiver 2.

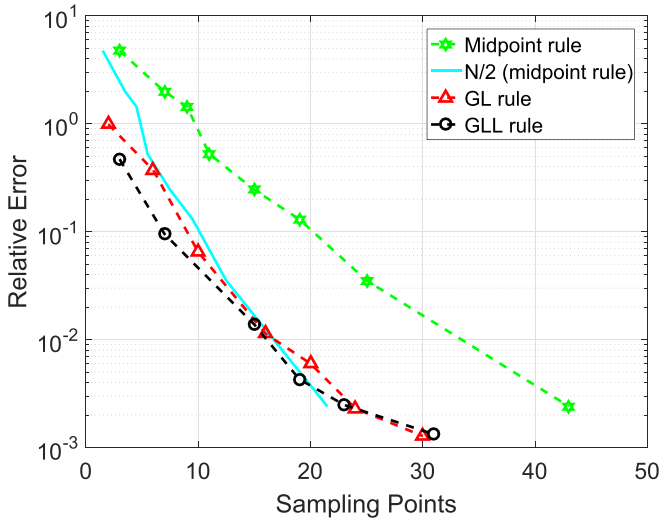

Fig. 6. The accuracy of the calculated field value H_x at receiver 1 obtained by midpoint rule (dashed line with star), GL rule (dashed line with triangle) and GLL rule (dashed line with circle). The solid line represents half of the sampling points by midpoint rule.

5. Examples

By solving a sequence of sparse linear equations and implementing GL rule to accelerate inverse Fourier transform, the electromagnetic fields at the receiver can be obtained in an efficient way. For triaxial logging tool, one can apply direct sparse solver to solve the linear system equation with three right-hand side excitations, representing *x*-, *y*- and *z*-directed magnetic dipole at the location of transmitter, respectively. In this way, one can acquire all the responses for one logging point simultaneously. Numerical examples of 1D transverse isotropic (TI) model, 1D fully anisotropic model and a realistic 2.5D model are given in this section.

5.1. Validation

Firstly, the scheme of 2.5D FDM modeling discussed in previous sections can be easily applied to model 1D structure. The scheme has been thoroughly tested, compared and validated against 1D analytical solution. Fig. 7 shows the formation of the 1D model with

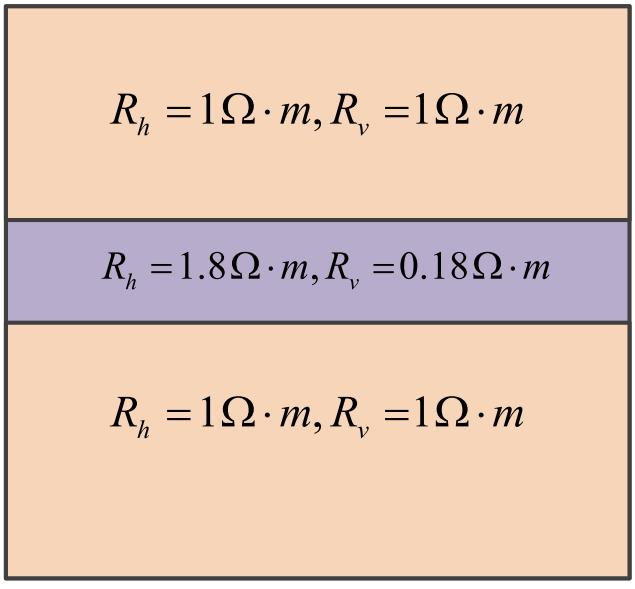

Fig. 7. The 1D model consisting of three transverse isotropic layers.

Table 1
CPU time and relative error of 2.5D FDM for modeling a three-layer TI formation shown in Fig. 7. The number of GL points is fixed at 20.

T-R spacing	2.5D grids	CPU time	Relative error
0.56 m	81 × 101	22.2 s	1.3%
0.56 m	99 × 140	38.6 s	0.46%
1.12 m	67 × 90	17.7 s	1.3%
1.12 m	85 × 131	30.3 s	0.77%

three horizontal layers. The layer in the middle has a thickness of 1.2 m. The horizontal resistivity R_h and vertical resistivity R_v in each layer are also shown. Situations with T-R spacings of 0.56 m and 1.12 m are simulated. Frequency of the source is 2 MHz. Table 1 summarizes the grid discretization, the CPU time and relative error with respect to analytical solutions based on 1D model, when the source is in the center of the middle layer and the tool is vertical placed. The total number of quadrature points is 20. This example suggests that the 2.5D FDM modeling can achieve a high accuracy. Generally speaking, a denser grid can bring better accuracy but also cost more computation time. The typical simulation time for one logging point is around half a minute.

To investigate the validity of 2.5D FD scheme to model fully anisotropic media, we implemented the scheme to study a three-layered formation as shown in Fig. 8, whose formation the 1D code can not model. Within each layer, the conductivity tensor is fully anisotropic. The tool runs in the formation at a dip angle of 15°. The center of the middle layer with thickness of 1.22 m locates at $z = 5$ m plane. The receiver is behind the transmitter with a T-R spacing of 0.51 m. The frequency of current source at the transmitter is 2 MHz. Fig. 9 shows the results of 2.5D FDM modeling and COMSOL software which uses 3D FEM. In the figures, H_{ij} $(i, j = x, y, z)$ means the *j*-component of magnetic field at the receiver due to the *i*-directed unit magnetic dipole at the transmitter. The results simulated by 2.5D FDM modeling agree very well with COMSOL. What's more, the field variations around the boundaries obtained by 2.5D FDM modeling match the results of 3D COMSOL in a good manner. In fact, the average relative error is around 1% which is sufficiently small for practical applications. All the simulations are conducted on an Intel Core i7 3.2-GHz processor. The numbers of grids in the *y* and *z* directions are about 70 and 110, respectively. And the number of quadrature points in the k_x domain is 20. For one logging point, the 2.5D FDM takes about 30 s while 3D COMSOL takes about 120 s to solve.

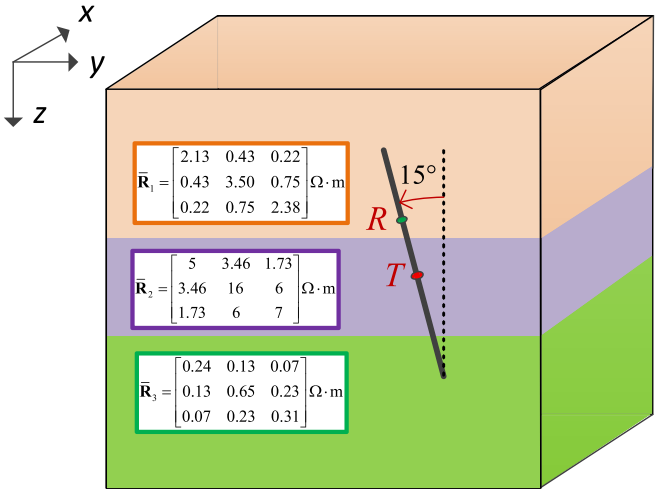

Fig. 8. A 1D model consisting of three fully anisotropic layers. The logging tool has a dip angle of 15°. The T-R spacing is 0.51 m.

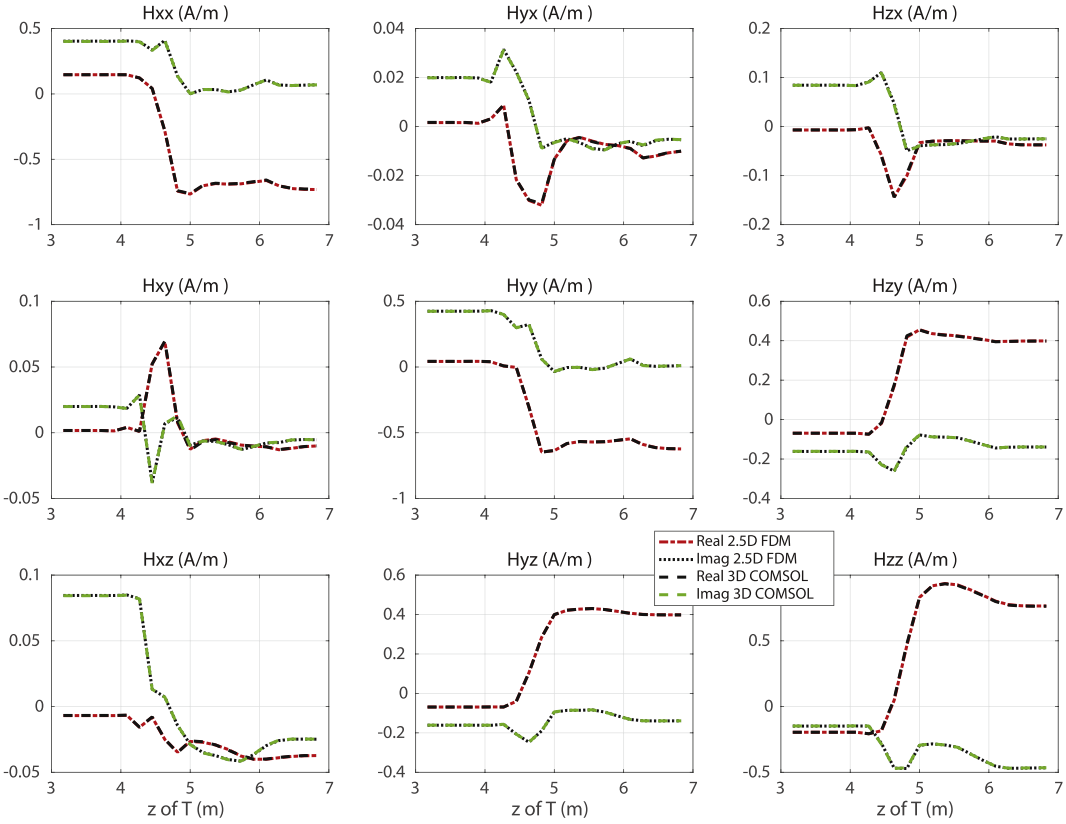

Fig. 9. Simulation results of the 1D model as shown in Fig. 8 by 3D FEM and 2.5D FD scheme.

5.2. Synthetic log simulation in a 2D formation with fault

The goal of previous examples is to validate the accuracy and efficiency of the 2.5D FDM scheme. To further validate the 2.5D FDM scheme solving six components of EM fields simultaneously, a complicated 2D example has been studied. Fig. 10 shows the geological formation to be studied. It consists three layers with a fault existing at the middle vertical line ($x = 0$ and $y = 0$). Each layer is filled with one material shown in Fig. 10 with the center layer is fully anisotropic. The resistivity tensor of each layer are shown in Fig. 10. The thicknesses of center layers are both 3.048 m. The vertical distance between center layers of left side and right side is 6.096 m. The trajectory of the tool is shown as black line running through the formation from left top to right bottom with a dip angle of 30°. The T-R spacings are 0.61 m and 1.17 m, respectively. The receivers are behind the transmitter. The working frequency of the tool is 400 kHz. Figs. 11 and 12 show the results obtained by 2.5D FDM modeling and by COMSOL whose solver is 3D FEM. The results obtained by 2.5D FDM modeling agree very well with those by COMSOL. The average relative error for this example is on the level of 1%, which is sufficiently small for most practical applications. In all the simulations for the 2D formation, the total number of grids is 8000–12,000. The number of quadrature points in the k_x domain is 20. For one logging point, the 2.5D FDM takes about 30 to 50 s while 3D COMSOL takes about 550 s to solve.

6. Conclusions

In this paper, we presented an efficient FDM scheme to model 2.5D problem in application of resistivity well logging tools. The electric and magnetic fields are solved simultaneously in order to assimilate the fully anisotropy in a straightforward way. Material average method is applied to fit the FDM solver with the staggered Yee's grid. We also applied Gaussian quadrature rules to speed up the inverse Fourier transform. In general, the accuracy of 2.5D FDM scheme is suitable for practical applications and the computational efficiency is much higher than 3D modeling. The proposed 2.5D FDM scheme will be promising in modeling and inversion of resistivity well logging in complex subsurface formation.

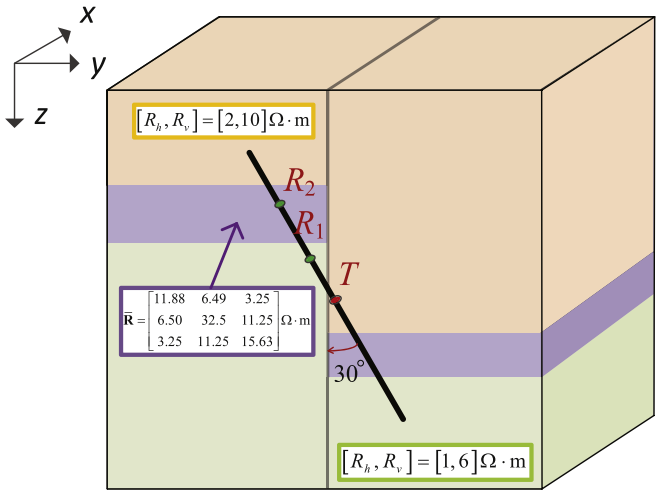

Fig. 10. A complicated 2D model with fault. The tool has a dip angle of 30°. The spacings between T and R_1 is 0.61 m and the spacing between T and R_2 is 1.17 m.

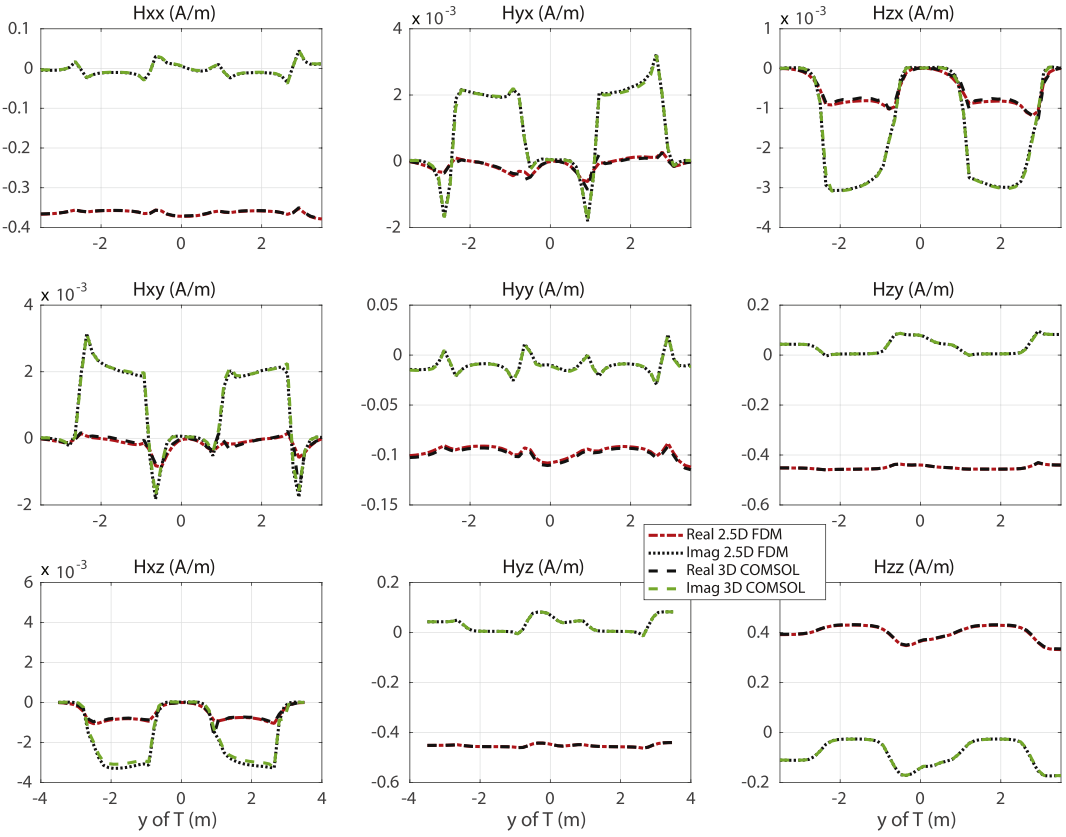

Fig. 11. Simulation results of the 2.5D model as shown in Fig. 10 by 3D FEM and 2.5D FD scheme. The T-R spacing is 0.61 m.

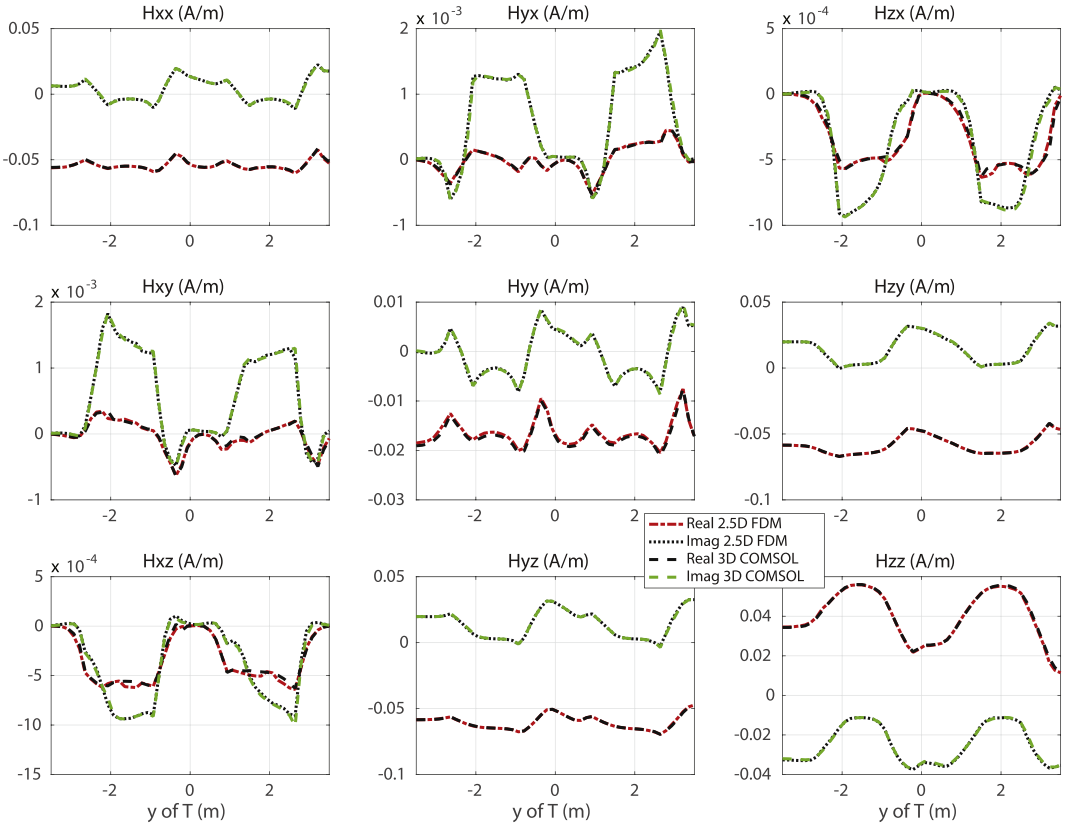

Fig. 12. Simulation results of the 2.5D model as shown in Fig. 10 by 3D FEM and 2.5D FD scheme. The T-R spacing is 1.17 m.

References

Abubakar, A., van Den Berg, P.M., Habashy, T.M., 2006a. An integral equation approach for 2.5-dimensional forward and inverse electromagnetic scattering. Geophys. J. Int. 165, 744–762. https://doi.org/10.1111/j.1365-246X.2005.02816.x.

Abubakar, A., Habashy, T., Druskin, V., Alumbaugh, D., Zerelli, A., Knizhnerman, L., 2006b. Two-and-half-dimensional forward and inverse modeling for marine CSEM problems. SEG Technical Program Expanded Abstracts 2006. pp. 750–754. https://doi.org/10.1190/1.2370366.

Abubakar, A., Habashy, T., Druskin, V., Alumbaugh, D., Zhang, P., Wilt, M., Denaclara, H., Nichols, E., Knizhnerman, L., 2005. A fast and rigorous 2.5D inversion algorithm for cross-well electromagnetic data. SEG Technical Program Expanded Abstracts 2005. Society of Exploration Geophysicists., pp. 534–537.

Abubakar, A., Habashy, T., Druskin, V., Knizhnerman, L., Alumbaugh, D., 2008. 2.5D forward and inverse modeling for interpreting low-frequency electromagnetic measurements. Geophysics 73, F165–F177. https://doi.org/10.1190/1.2937466.

Anderson, W.L., 1979. Numerical integration of related Hankel transforms of orders 0 and 1 by adaptive digital filtering. Geophysics 44, 1287–1305. https://doi.org/10.1190/1.1441007.

Avdeev, D.B., 2005. Three-dimensional electromagnetic modelling and inversion from theory to application. Surv. Geophys. 26, 767–799. https://doi.org/10.1007/s10712-005-1836-x.

Bittar, M., Aki, A., 2015. Advancement and economic benefit of geosteering and well-placement technology. Lead. Edge 34, 524–528. https://doi.org/10.1190/tle34050524.1.

Bittar, M.S., Klein, J.D., Randy, B., Hu, G., Wu, M., Pitcher, J.L., Golla, C., Althoff, G.D., Sitka, M., Minosyan, V., et al. 2009. A new azimuthal deep-reading resistivity tool for geosteering and advanced formation evaluation. SPE Reserv. Eval. Eng. 12, 270–279. https://doi.org/10.2118/109971-PA.

Chen, J., Wang, J., Yu, Y., 2016. An improved complex image theory for fast resistivity modeling and its application to geosteering. SPE J. 21, 1450–1457. https://doi.org/10.2118/170661-PA.

Chen, Y.-H., Omeragic, D., Druskin, V., Kuo, C.-H., Habashy, T., Abubakar, A., Knizhnerman, L., 2011. 2.5D FD modeling of EM directional propagation tools in high-angle and horizontal wells. SEG Technical Program Expanded Abstracts 2011. Society of Exploration Geophysicists., pp. 422–426. https://doi.org/10.1190/1.3628090.

Davis, T.A., 2006. Direct Methods for Sparse Linear Systems. SIAM.

Davis, T.A., Duff, I.S., 1997. An unsymmetric-pattern multifrontal method for sparse LU factorization. SIAM J. Matrix Anal. Appl. 18, 140–158. https://doi.org/10.1137/S0895479894246905.

Davydycheva, S., 2010. 3D modeling of new-generation (1999–2010) resistivity logging tools. Lead. Edge 29, 780–789. https://doi.org/10.1190/1.3462778.

Davydycheva, S., Druskin, V., Habashy, T., 2003. An efficient finite-difference scheme for electromagnetic logging in 3D anisotropic inhomogeneous media. Geophysics 68, 1525–1536. https://doi.org/10.1190/1.1620626.

Dyatlov, G., Kushnir, D., Dashevsky, Y., 2017. Treatment of singularity in the method of boundary integral equations for 2.5D electromagnetic modeling. Geophysics 82, E57–E75. https://doi.org/10.1190/geo2015-0645.1.

Dyatlov, G., Onegova, E., Dashevsky, Y., 2015. Efficient 2.5D electromagnetic modeling using boundary integral equations. Geophysics 80, E163–E173. https://doi.org/10.1190/geo2014-0237.1.

He, Z., Liu, R.C., Huang, K., Guo, C., 2015. A fast algorithm to forward model the triaxial induction logging response in layered transversely isotropic dipping formations. Geophysics 80, D237–D245. https://doi.org/10.1190/geo2014-0321.1.

Hou, J., Mallan, R.K., Torres-Verdín, C., 2006. Finite-difference simulation of borehole EM measurements in 3D anisotropic media using coupled scalar-vector potentials. Geophysics 71, G225–G233. https://doi.org/10.1190/1.2245467.

Huang, M., Shen, L.C., 1989. Computation of induction logs in multiple-layer dipping formation. IEEE Trans. Geosci. Remote Sens. 27, 259–267. https://doi.org/10.1109/36.17667.

Hursan, G., Zhdanov, M.S., 2002. Contraction integral equation method in three-dimensional electromagnetic modeling. Radio Sci. 37.

Jaysaval, P., Shantsev, D.V., de la Kethulle de Ryhove, S., Bratteland, T., 2016. Fully anisotropic 3-D EM modelling on a lebedev grid with a multigrid pre-conditioner. Geophys. J. Int. 207, 1554–1572. https://doi.org/10.1093/gji/ggw352.

Jin, J.-M., Zunoubi, M., Donepudi, K.C., Chew, W.C., 1999. Frequency-domain and time-domain finite-element solution of Maxwell's equations using spectral Lanczos decomposition method. Comput. Methods Appl. Mech. Eng. 169, 279–296. https://doi.org/10.1016/S0045-7825(98)00158-3.

Key, K., 2016. MARE2DEM: a 2-D inversion code for controlled-source electromagnetic and magnetotelluric data. Geophys. J. Int. 207, 571–588. https://doi.org/10.1093/gji/ggw290.

Key, K., Ovall, J., 2011. A parallel goal-oriented adaptive finite element method for 2.5-D electromagnetic modelling. Geophys. J. Int. 186, 137–154. https://doi.org/10.1111/j.1365-246X.2011.05025.x.

Kong, F., Johnstad, S., Røsten, T., Westerdahl, H., 2007. A 2.5D finite-element-modeling difference method for marine CSEM modeling in stratified anisotropic media. Geophysics 73, F9–F19. https://doi.org/10.1190/1.2819691.

Lebedev, V.I., 1964. Difference analogies of orthogonal decompositions of basic differential operators and some boundary value problems. I (Russian). Sov. Comput. Math. Math. Phys. 4, 449–465.

Li, Q., Omeragic, D., Chou, L., Yang, L., Duong, K., et al. 2005. New directional electromagnetic tool for proactive geosteering and accurate formation evaluation while drilling. SPWLA 46th Annual Logging Symposium. Society of Petrophysicists and Well-Log Analysts.

Li, Y., Key, K., 2007. 2D marine controlled-source electromagnetic modeling: part 1–an adaptive finite-element algorithm. Geophysics 72, WA51–WA62. https://doi.org/10.1190/1.2432262.

Liu, Y., Yin, C., 2014. 3D anisotropic modeling for airborne EM systems using finite-difference method. J. Appl. Geophys. 109, 186–194. https://doi.org/10.1016/j.jappgeo.2014.07.003.

Martí, A., 2014. The role of electrical anisotropy in magnetotelluric responses: from modelling and dimensionality analysis to inversion and interpretation. Surv. Geophys. 35, 179–218. https://doi.org/10.1007/s10712-013-9233-3.

Nam, M.J., Pardo, D., Torres-Verdín, C., 2012. Simulation of borehole-eccentered triaxial induction measurements using a Fourier hp finite-element method. Geophysics 78, D41–D52. https://doi.org/10.1190/geo2011-0524.1.

Omeragic, D., Habashy, T., Chen, Y.-H., Polyakov, V., Kuo, C.-h., Altman, R., Hupp, D., Maeso, C., 2009. 3D reservoir characterization and well placement in complex scenarios using LWD directional EM measurements. Petrophysics 50, 396–415.

Quarteroni, A., Sacco, R., Saleri, F., 2010. Numerical Mathematics. vol. 37. Springer Science & Business Media.

Wang, T., Fang, S., 2001. 3-D electromagnetic anisotropy modeling using finite differences. Geophysics 66, 1386–1398. https://doi.org/10.1190/1.1486779.

Weidelt, P., 1999. 3-D conductivity models: implications of electrical anisotropy. Three-dimensional Electromagnetics, 7. , pp. 119–137.

Weiss, C.J., Newman, G.A., 2002. Electromagnetic induction in a fully 3-D anisotropic earth. Geophysics 67 (4), 1104–1114. https://doi.org/10.1190/1.1500371.

Yee, K., 1966. Numerical solution of initial boundary value problems involving Maxwell's equations in isotropic media. IEEE Trans. Antennas Propag. 14, 302–307. https://doi.org/10.1109/TAP.1966.1138693.

Zhdanov, M.S., Lee, S.K., Yoshioka, K., 2006. Integral equation method for 3D modeling of electromagnetic fields in complex structures with inhomogeneous background conductivity. Geophysics 71, G333–G345. https://doi.org/10.1190/1.2358403.

Zhong, L., Li, J., Bhardwaj, A., Shen, L.C., Liu, R.C., 2008. Computation of triaxial induction logging tools in layered anisotropic dipping formations. IEEE Trans. Geosci. Remote Sens. 46, 1148–1163. https://doi.org/10.1109/TGRS.2008.915749.

Zhou, J., 2015. Uncertainty in geosteering and interpretation of horizontal wells — the necessity for constraints and geometric models. Lead. Edge 34, 492–499. https://doi.org/10.1190/tle34050496.1.